

A Derivation of the Analytical Relationship between the Projected Albedo-Area Product of a Space Object and its Aggregate Photometric Measurements

Tamara E. Payne, Keith Lucas, Anil Chaudhary, Shaylah Mutschler

Applied Optimization Inc.

Phan Dao, Jeremy Murray-Krezan

Air Force Research Laboratory/RVBY

ABSTRACT

In this paper, we present a method to directly convert the photometric measurements to the projected albedo-Area product of a resident space object. The derivation is based on Lambertian reflectance but is general in all other ways. Its most powerful attribute is that it is independent of sensor, space object geometry and other characteristics, as well as photometric waveband. The governing expression can be combined with specific geometries of different orbits and satellite attitude control methods to obtain a parent equation from which the component projected albedo-Area products can be calculated.

First we develop the governing expression from first principals and provide its physical and mathematical foundations. Then we derive, for the specific case of a three-axis stabilized satellite with a nadir-pointing body and articulating solar panels, the parent equation for the unique geometries of this case. Then we show how to decompose the aggregate albedo-Area product of the satellite into the respective albedo-Area products of the body and the solar panels.

The governing albedo-Area expression provides a baseline that can be utilized for the characterization of a variety of space objects irrespective of their geometry and attitude.

1.0 INTRODUCTION

Objects in deep space, especially those in geosynchronous orbit, present challenges to electro-optical and radar technologies. One of the biggest challenges is to characterize objects that are spatially non-resolvable by either technology. There are a few features that are readily extracted from the reflected solar illumination off of the objects. If the object is tumbling or spinning, variations in the brightness can be used to compute the spin period and spin axis [1]. If the object is three-axis stabilized, variations in the brightness can be used to classify the object by signature type [2]. The time-scales over which these variations occur are typically very different for these two cases. Unstable or spin-stabilized objects vary on the timescales of minutes while three-axis stabilized objects vary on the timescales of hours. However, in the latter case, there is much work ahead to understand the variations in brightness as they relate to the satellite body and solar panel physical attributes. To this end, we work from first principals to derive equations for decomposing the aggregate reflectance of a three-axis stabilized object by considering the nadir pointing parts of the object as one facet (termed the “body”) and the solar tracking parts of the object as another facet (termed the solar panels). This comprises the two-facet model [3].

Presently we are not merely content with using the brightness data per se as a characteristic feature, but wish to extract more information from the brightness data relevant to physical properties of the object itself. The reflected brightness of an object is dependent on two intrinsic properties; the albedo of the surface materials and the projected area visible to the observer. These traits are intertwined and cannot be separated without data complimentary to the brightness data. However their product, albedo-Area, can be directly extracted from the brightness data.

The main objective of this paper is to show the derivation of the calculations that decompose the total photometric signature into component panel and body albedo-Areas. To that end, the construction of the two-facet model is explained, providing an overview of the geometry and the Bidirectional Reflectivity Distribution Function (BRDF) employed. The derivation of the total albedo-Area from its photometric signature is provided, and, lastly, the total projected albedo-Area’s decomposition into the component panel and body albedo-Areas is explained. A second objective of this paper is to provide an explanation of the physical and mathematical foundations of the work. Since the laws that govern reflectance photometry and radiometry which underlie this work are gathered from a variety of sources, it is often difficult (or at least time consuming) to find the relevant, disparate pieces of information.

Accordingly, this paper is meant to fill this gap by aggregating the concepts germane to the conversion of brightness data into albedo-Area.

This paper is organized as follows. First we start our discussion in Section 2.0 by reviewing the definitions of intensity and flux and the relationship between them. Next, the fundamental concepts and assumptions used in the model are presented in Section 3.0. In Section 4.0, we present the derivation of the projected albedo-Area equation. Then in Section 5.0, we examine the body component to set up how the aggregate albedo-Area is decomposed to solve for the body and panel albedo-Areas separately, which is discussed in Section 6.0. Finally the conclusions are presented in Section 7.0.

2.0 PRELIMINARY CONSIDERATIONS

Before preceding further, the definitions of *intensity* and *flux*, as laid out in Henden's and Kaitchuck's *Astronomical Photometry*, are presented [4]. This is done to justify the relationship between intensity and flux used in the derivation. Although these terms are based in emissive radiometry, they are the foundation for the reflectance equations when considering an unresolved point source. Please note the scope of variables defined in this section does not extend to subsequent sections. In other words, the definition of several symbols used here is limited to this section only.

2.1 INTENSITY

First, recall that a *steradian* is the central solid angle of a sphere of radius r subtended by an area on the sphere equal to r^2 (note that the shape of the area is irrelevant, but often considered circular or rectilinear). Since the surface area of a sphere is $4\pi r^2$, there are 4π steradians in a sphere. This means that the volume of one steradian is $\frac{1}{4\pi}$ of the total volume of the sphere that subtends it. Furthermore, since one steradian is the ratio between an area and the square of the radius, both having dimension *length*², the steradian is unitless. The symbol *sr*, however, is used to denote steradians for bookkeeping.

Intensity, then, is the total energy in a certain waveband flowing through a solid angle subtended by an area on the source. If a source is radiating evenly, for instance, one steradian central solid angle would contain $\frac{1}{4\pi}$ of the total energy radiated. Consider Fig. 2-1, adapted from the text [4].

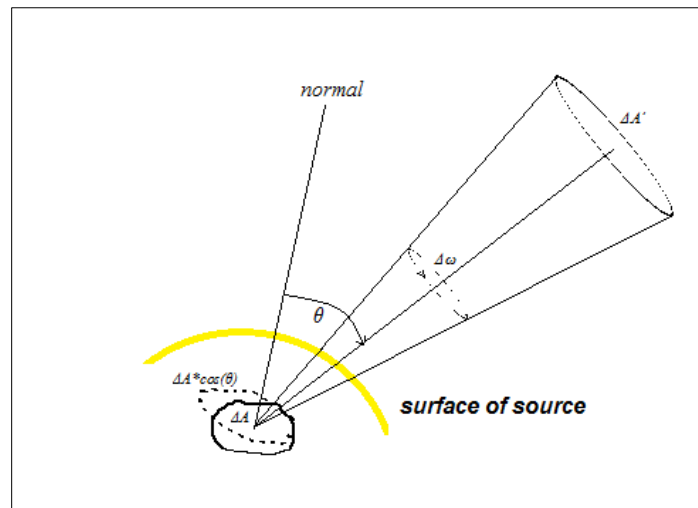


Fig. 2-1. Intensity Observed from a Source

ΔA is an area on the surface of the source. As $\Delta A \rightarrow 0$, it becomes a small area subtending the solid angle $\Delta\omega$ infinitesimally close to the vertex, while $\Delta\omega$ may be offset from the surface normal by angle θ (depending on the orientation of the observer). In the case that $\theta = 0$, an observer peering down the axis of $\Delta\omega$ would observe the actual area ΔA . As $\theta \rightarrow 90^\circ$, however, the apparent area (and therefore the observed intensity) approaches zero. One may visualize this concept by holding a flat object face-on and then slowly rotating it so that it is eventually edge-on. It is the projected area, $\Delta A \cdot \cos(\theta)$, that is of importance.

Intensity, in more detail, is the total energy ΔE in a certain waveband flowing from a source into a solid angle $\Delta\omega$ from a projected area $\Delta A \cdot \cos(\theta)$ over time Δt , where ΔE is proportional to $\Delta\omega$, $\Delta A \cdot \cos(\theta)$, and Δt . Intensity I is then defined as the ratio of these quantities as they tend to zero, as shown next in (2-1).

$$I = \lim_{\substack{\Delta E \rightarrow 0 \\ \Delta\omega \rightarrow 0 \\ \Delta A \rightarrow 0 \\ \Delta t \rightarrow 0}} \left[\frac{\Delta E}{\Delta\omega \Delta A \cos(\theta) \Delta t} \right] \quad (2-1)$$

$$\Downarrow$$

$$I = \frac{dE}{dt d\omega dA \cos(\theta)}$$

2.2 FLUX

Flux, on the other hand, is the measure of the net energy transfer in a certain waveband across an area over time [4]. As in Fig. 2-1, an area ΔA on the source is the threshold through which energy may enter or exit. *Flux*, then, is the net sum of the energy ΔE flowing both inward and outward through ΔA over time Δt . Recall that ΔE is proportional to ΔA and Δt . Flux f is then defined to be the sum as the quantities tend to zero, shown in (2-2).

$$f = \lim_{\substack{\Delta E \rightarrow 0 \\ \Delta A \rightarrow 0 \\ \Delta t \rightarrow 0}} \sum \frac{\Delta E}{\Delta A \cdot \Delta t} \quad (2-2)$$

$$\Downarrow$$

$$f = \frac{\int dE}{dA dt}$$

2.3 RELATIONSHIP BETWEEN INTENSITY AND FLUX

Solving for dE from (2-1), equation (2-3) is obtained.

$$dE = I dt d\omega dA \cos(\theta) \quad (2-3)$$

Substituting (2-3) into (2-2) and integrating over all angles, the following expression for flux in terms of intensity is obtained, shown next in (2-4).

$$f = \int_{\text{all angles}} I \cos(\theta) d\omega \quad (2-4)$$

Up to this point, the geometry of the situation has been viewed from the perspective of the “solid angle” convention. Although this is helpful for visualization, it is more convenient to convert to spherical coordinates when doing the actual integration. That conversion is now performed, followed by the computation of the flux-intensity integral.

Consider a spherical coordinate system in lieu of the solid angle convention, with $r = 1.0$, as shown in Fig. 2-2. Recall Fig. 2-1. Let the normal be the z axis, and let the xy plane lie tangent to the area ΔA . Let ω be the solid angle swept out by the angle θ off the z axis ranging from 0 to π and by the angle ϕ off the x axis in the xy plane ranging from 0 to 2π .

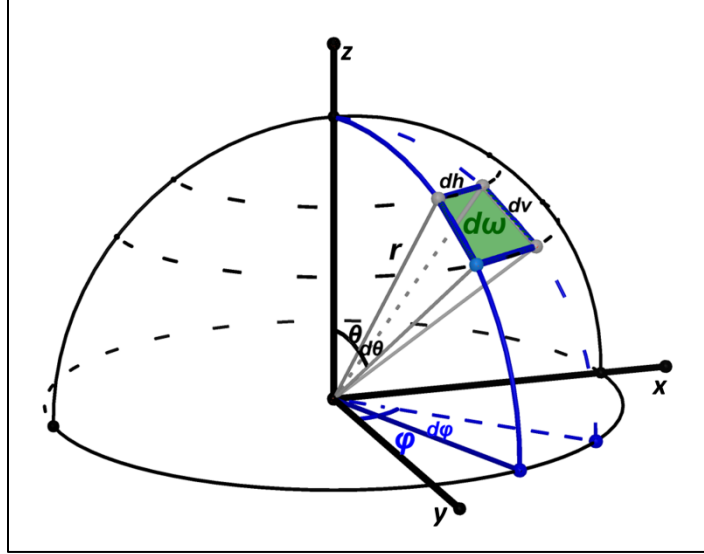


Fig. 2-2. Solid Angle Conversion to Spherical Coordinates

This solid angle ω , subtended by the unit sphere and forming a rectilinear casque, can now be differentiated in terms of spherical coordinates, as shown in (2-5).

$$\begin{aligned}
 d\theta &= dv \text{ and } d\phi = \frac{dh}{\sin(\theta)} \\
 &\Downarrow \\
 dh &= \sin(\theta) d\phi \\
 &\Downarrow
 \end{aligned}
 \tag{2-5}$$

$$d\omega = dv dh = \sin(\theta) d\theta d\phi$$

Substituting now for $d\omega$ in (2-4) and integrating over θ and ϕ , the following expression for flux, shown in (2-6), is obtained.

$$f = \int_0^{2\pi} \int_0^{\pi} I \cos(\theta) \sin(\theta) d\theta d\phi \tag{2-6}$$

Equation (2-6) can now be broken up into the component energies moving inward and outward from the surface, as shown next in (2-7).

$$f = \int_0^{2\pi} \int_0^{\frac{\pi}{2}} I_{OUT} \cos(\theta) \sin(\theta) d\theta d\phi + \int_0^{2\pi} \int_{\frac{\pi}{2}}^{\pi} I_{IN} \cos(\theta) \sin(\theta) d\theta d\phi \tag{2-7}$$

Since only the flux outward from the source is considered, the inward contribution is zeroed out, as shown in (2-8).

$$f = \int_0^{2\pi} \int_0^{\frac{\pi}{2}} I \cos(\theta) \sin(\theta) d\theta d\phi \tag{2-8}$$

Furthermore, assuming I does not depend on any angle (which is true only in the Lambertian reflectance case), it may be factored out. The integral is now directly computed in (2-9).

$$\begin{aligned}
 f &= \pi I \\
 &\Downarrow \\
 I &= \frac{1}{\pi} f
 \end{aligned}
 \tag{2-9}$$

It has now been established that, in the Lambertian case and at the source before radiating outward, flux is proportional by a factor of π to intensity [4]. Equation (2-9) will be invoked when the equation for the projected albedo-Area of the space object is derived.

3.0 FUNDAMENTALS

In this section, the prerequisite theory and assumptions underlying the model are outlined, and the definitions of specific terms and angles are provided. This section ends with the derivation of the total reflected intensity equation, which is the foundation for the total albedo-Area equation derived in Section 4.0.

3.1 ASSUMPTIONS

1. The space object has a *three-axis stabilized, nadir-pointing body*.
2. The space object has *sunward facing, articulating solar panels*.
3. The space object is represented by a *two-facet model* in which one facet represents the solar panels and the other represents the body.
4. The panel facet is approximately planar and possesses both *specular* and *Lambertian* reflectance properties. Because it tends to zero away from the vector of specular reflection (glint), the specular component is only dominant within a glint region. Otherwise, the panel reflectance is dominated by Lambertian reflectance.
5. The body is a complex three-dimensional shape with approximately Lambertian aggregate reflectance. Its albedo-Area is pose-dependent and is more accurately represented by a series of values rather than by a single value.

3.2 “PROJECTED” VS. “INTRINSIC” ALBEDO-AREA

The *albedo-Area* (aA) of an object is the product of its *albedo*, the ratio of the electro-magnetic radiation reflected by an object to the amount that is incident on it, with its area. Since albedo is a ratio of quantities of equivalent dimension, it is unit-less. The aA then, is reported in units of area, [m^2].

While aA is a property that is intrinsic to an object, the observed aA of an object at any given moment is a projection of its geometry of observation with respect to the source of illumination and the sensor. “*Projected*” aA of an object, then, refers to its observed value based on the current geometry of the observation. “*Intrinsic*” aA of an object, on the other hand, refers to its value independently of the geometry of observation.

For clarity, the symbol \widetilde{aA}_x is used to represent an object x 's projected aA , while the symbol \mathbf{aA}_x is used to represent its intrinsic aA .

3.3 ANGLES OF POSE AND OBSERVATION

The term *angle of pose* refers to any angle that describes the object's position with respect to the earth and the sun. The angle of pose is defined independently of the observer position. Examples of angles of pose include longitudinal and latitudinal phase angles and *orbital angle*, an angle analogous to longitudinal phase angle that is described in detail in this section.

The term *angle of observation* refers to any angle that is defined in reference to the space object and its observer. Examples of this type of angle include the angle between the sun, space object (vertex), and observer or the angle between the space object – observer vector and the panel surface normal.

3.3.1 Angles of Observation

Consider Fig. 3-1, an illustration of a Resident Space Object (RSO) with a three-axis stabilized, nadir-pointing body component and an articulating, sunward facing solar panel component. The sun is the orange sphere, the earth is the blue sphere, the observer is the small purple sphere, the solar panel is the green square, and the body is the blue cube. The vector N is normal to the orbital plane of the satellite. In other words, it is orbital north. The solar panel pivots about the orbital north vector to maintain a sunward-facing orientation.

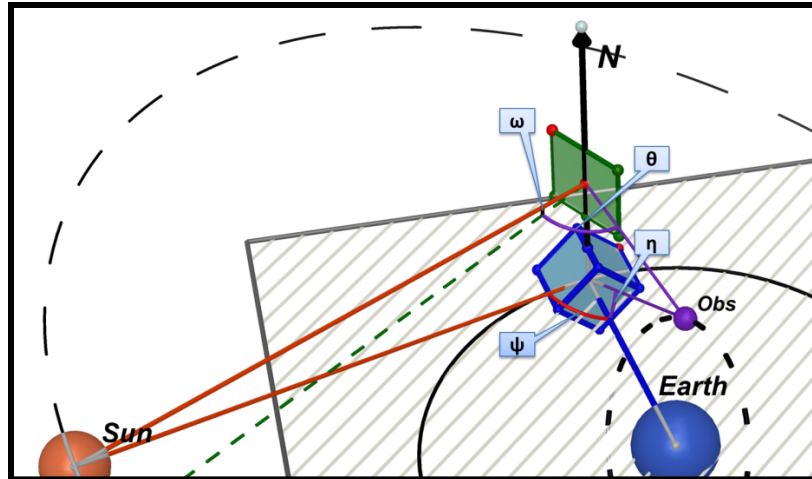


Fig. 3-1. Space Object Angles of Observation (not to scale)¹. The blue cube represents the body and the green square represents the solar panel.

The angles θ and ω are the main angles of observation for the solar panel. Angle θ is the angle between the observer-RSO vector and the panel normal vector, and it determines the panel's projected area from an observer's point of view. Angle ω is the angle between the RSO-sun vector and the panel normal vector, and it determines the panel's projected brightness per unit area.

The angles ψ and η are the main angles of observation for the body component. Angle ψ is the angle between the RSO-sun vector and the RSO-Earth vector, and it determines the projected brightness per unit area of the body's nadir-pointing face. Angle η is the angle between the RSO-Earth vector and the observer-RSO vector, and it determines the projected area of the body's nadir-pointing face from the observer's point of view.

Consider now Fig. 3-2, an illustration of the panel by itself. This figure depicts the panel from its self-centered frame of reference. The sun is the orange sphere. The panel is the green square. The dashed green line is normal to the panel. The purple line is the RSO-observer vector. The N vector (aligned with the orbital north) is shown as a dotted black line. The N vector and panel normal define the third axis of the orthogonal triad, which is also depicted as a dotted black line. The angle between the RSO-sun vector (orange line) and the panel normal (dotted green line) is ω . The specular reflection of the incident sunlight takes place along the pink vector, and the angle between it and the panel normal vector is congruent to ω .

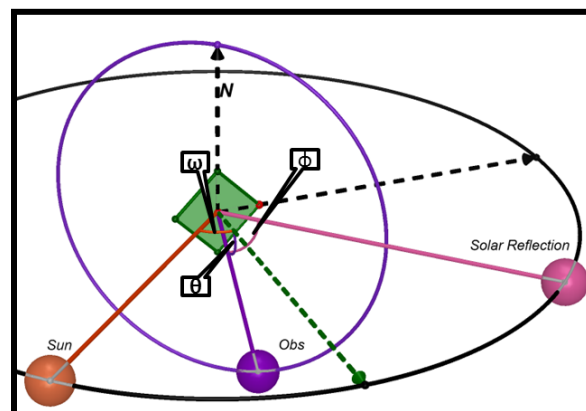


Fig. 3-2. Solar Panel Centered Frame of Reference

¹ Note that although the vectors between the sun and solar panel and the sun and body appear to be different (both in orange), they are essentially the same vector when considered at the true scale.

The angle ϕ is defined to be the angle between the observer-RSO vector (purple) and the specular reflection vector of the sun (pink). This angle is important in determining when a panel enters the *glint region* in which the panel's specular reflectance dominates its Lambertian reflectance. When angle ϕ is equal to 0° , for instance, the observer's line of sight is aligned with the solar specular reflection, and the observer will detect a glint of maximum brightness.

3.3.2 Angles of Pose

The angles of pose to consider are the space object's longitudinal and latitudinal phase angles, along with its *orbital angle*. While the two former angles are from an Earth-centered reference frame, the latter is defined from the perspective of the space object and is observer independent. Since, in the space-based case, the observer is in motion relative to the space object, defining such an angle simplifies the geometry of the situation. Consider the illustration of orbital angle in Fig. 3-3.

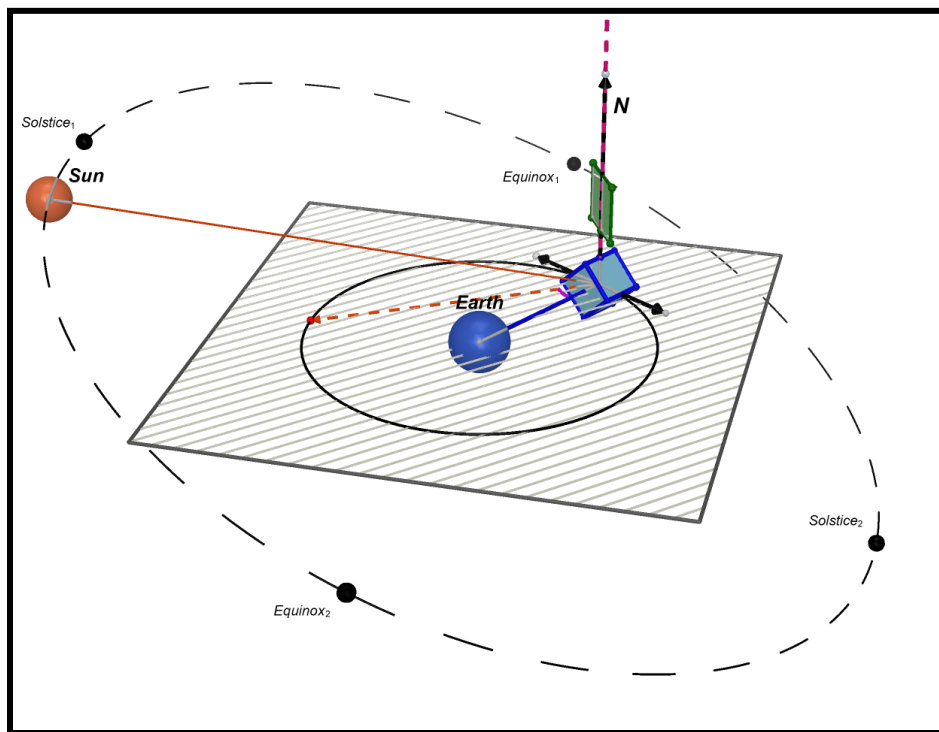


Fig. 3-3. Definition of Orbital Angle (γ). The orbital angle is the angle between the solid blue line (RSO-Earth vector) and the dashed orange line (projection of the RSO-sun vector onto the orbital plane of the space object).

The orbital angle is defined as the signed angle between the RSO-Earth vector and the projection of the RSO-sun vector onto the orbital plane. In Fig. 3-3, the RSO-Earth vector is shown as a solid blue line. The orbital plane is the square with gray hatch marks. The dashed orange line is the projection of the RSO-sun vector onto the orbital plane. The orbital angle is the angle between the dashed orange line and the blue line, marked as a purple arc. It ranges over the interval $(-\frac{\pi}{2}, \frac{\pi}{2})$ for visible objects and is denoted as γ when used in Section 5.3. The orbital angle calculation is performed directly using the orthogonal reference frame centered at the RSO, in which the z-axis is orbital north (the vector perpendicular to the orbital plane).

The orbital angle changes sign where the direction of the cross product between the RSO-sun vector projection onto the orbital plane and the RSO-Earth vector changes by the right-hand rule. It is defined positive when the cross product aligns with orbital north and negative otherwise.

3.4 REFLECTED INTENSITY OF THE RSO

The reflected intensity of the object's total reflection is the sum of the panel and body component reflected intensities, as written in (3-1).

$$I_{RSO} = I_P + I_B [W/sr] \tag{3-1}$$

Consider now the panel component separately. The panel's reflected intensity is the sum of both specular and Lambertian components, as written in (3-2).

$$I_p = I_{pS} + I_{pL} \text{ [W/sr]} \quad (3-2)$$

Recall the previously defined angles and vectors, reprinted for convenience in Fig. 3-4.

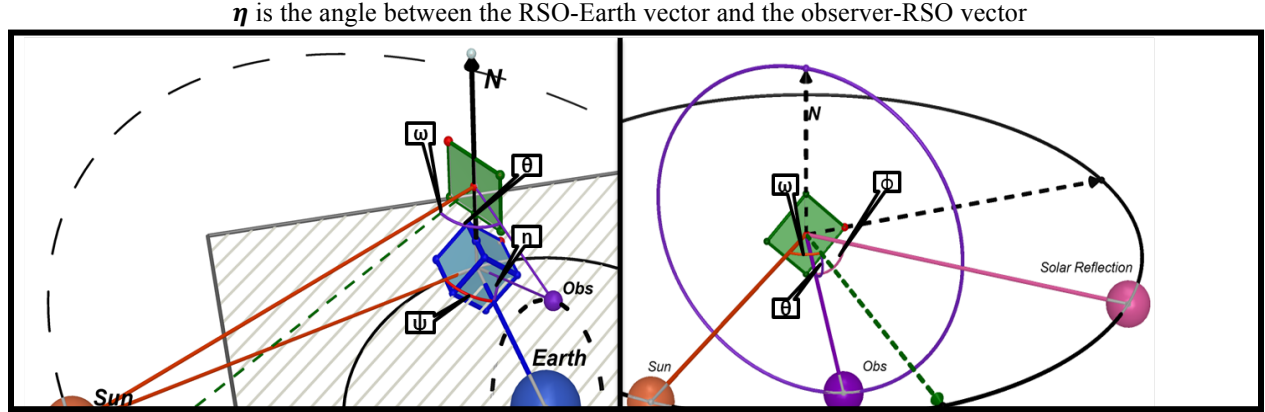


Fig. 3-4. Angles and Vectors Recap

From the observer's perspective, the specular component I_{pS} of the panel is proportional to the Phong specular reflectance term of $\cos^m(\phi)$, where ϕ is the angle between the observer-RSO vector and the solar reflection vector (note that m is the specularity exponent per the Phong model). The specular component is also proportional to the projected area of the panel, contributing a factor of $\cos(\theta)$, where θ is the angle between the observer-RSO vector and the panel surface normal vector. As angle ϕ becomes large, $\cos^m(\phi)$ approaches 0 and the specular term can be ignored. However, as angle ϕ approaches 0, $\cos^m(\phi)$ becomes much more dominant, and a glint occurs. At $\phi = 0^\circ$, the observer is directly in line with the specular reflection of the panel, and a maximal glint is detected.

The Lambertian component I_{pL} of the panel is proportional to its projected brightness, contributing a factor of $\cos(\omega)$, where ω is the angle between the RSO-sun vector and the panel surface normal vector. It is also proportional to its projected area, contributing a factor of $\cos(\theta)$. For large values of ϕ , ($\cos^m(\phi)$ approaches 0), Equation (3-2) may be approximated as (3-3).

$$I_p \approx I_{pL} \cos(\omega) \cos(\theta) \text{ [W/sr]} \quad (3-3)$$

Now consider the body component separately. The intensity of the body's reflection is assumed to be approximately Lambertian, as the body is an aggregate of many small facets. The body's intensity is proportional to the projected brightness of the body, contributing a factor of $\cos(\psi)$, where ψ is the angle between the RSO-sun vector and the RSO-Earth vector. It is also proportional to the projected area of the body, contributing a factor of $\cos(\eta)$, where η is the angle between the observer-RSO vector and the RSO-Earth vector.

Although the body is a complex three-dimensional shape and warrants a more detailed algebraic model to describe it, the following simplified expression for the body's reflected intensity shown in (3-4) is sufficient for the time being.

$$I_B = I_{BL} \cos(\psi) \cos(\eta) \text{ [W/sr]} \quad (3-4)$$

Equation (3-1) is now re-written in terms of (3-2) and (3-3) for large values of ϕ , where the panel's specular component becomes insignificant. The resulting Lambertian-only equation for the RSO's total reflected intensity is shown now in (3-5).

$$I_{RSO} = I_{pL} \cos(\omega) \cos(\theta) + I_{BL} \cos(\psi) \cos(\eta) \text{ [W/sr]} \quad (3-5)$$

4.0 PROJECTED ALBEDO-AREA EQUATION DERIVATION

The observation data sets include both photometric measurements of the space object, in terms of apparent magnitude, and astrometric measurements, in terms of Earth-Centered Inertial (ECI) coordinates for the space

object, sensor, and sun. From these data sets, a measurement of the RSO's albedo-Area as a projection of the observation geometry is calculated. In this section, the *projected albedo-Area equation* that provides the value of this measurement is derived.

4.1 MAGNITUDE, INTENSITY, AND FLUX

While the sensor reports photometric data in terms of apparent magnitude, the RSO's observed albedo-Area is a result of the reflected solar radiation in terms of incident solar flux. Equations relating apparent magnitude, radiant intensity and radiant flux are therefore required for the transformation of apparent magnitude into albedo-Area.

4.1.1 Intensity and Flux Relationship

Consider a point source of reflected light. At the point source, before the reflected electromagnetic energy propagates outward, (2-9) states that, in the Lambertian case, radiant intensity and radiant flux are directly proportional by a factor of π , reprinted here in (4-1).

$$\begin{aligned} I &= \frac{1}{\pi} f \\ \Downarrow \\ f &= \pi I \end{aligned} \tag{4-1}$$

Consider viewing the same point source now over a distance. The relationship between the radiant intensity and flux of that object, I and f , follows from the inverse square law of light, described next. As the reflected electromagnetic energy propagates outward from the point source in a solid angle over a distance R , its intensity decreases with the square of the distance traveled. Taking this relationship into account, (4-2) is obtained [5].

$$\begin{aligned} f \left[\frac{W}{sr \ m^2} \right] &= \frac{I \left[\frac{W}{sr} \right]}{R^2 [m^2]} \\ \Downarrow \\ I \cdot \left[\frac{W}{sr} \right] &= f \left[\frac{W}{sr \ m^2} \right] r^2 [m^2] \end{aligned} \tag{4-2}$$

4.1.2 Flux and Apparent Magnitude Relationship

Apparent magnitude is a unit-less measure of the brightness of a celestial object relative to that of another celestial object in a certain electromagnetic waveband. Considering the apparent magnitude of an object x relative to that of a reference object REF in a certain waveband, apparent magnitude and flux are related in the following way, as shown in (4-3) [4].

$$\begin{aligned} m_x - m_{REF} &= -2.5 \cdot \log_{10} \frac{f_x}{f_{REF}} \\ \Downarrow \\ \frac{f_x}{f_{REF}} &= 10^{\frac{m_{REF} - m_x}{2.5}} \end{aligned} \tag{4-3}$$

4.2 FOUNDATION FOR THE PROJECTED ALBEDO-AREA EQUATION

Recall (3-5), the reflected intensity equation, reprinted here for convenience in (4-4).

$$I_{RSO} = I_{PL} \cos(\omega) \cos(\theta) + I_{BL} \cos(\psi) \cos(\eta) [W/sr] \tag{4-4}$$

Recall also that I_{PL} and I_{BL} are Lambertian-only components of the panel's and body's reflectance. Next, the foundations of these components are described.

First, each component intensity is the result of the incident reflected solar radiation, so each component must be proportional to the incoming solar flux, $f_{sun} \left[\frac{W}{sr} \right]$, also known as the solar constant. Furthermore, since the component intensities are assumed Lambertian, the constant of proportionality is $\frac{1}{\pi}$, by (4-1).

Second, as this intensity is reflected off of a certain area, it is proportional to that area, $A [m^2]$.

Third, the amount of solar radiation reflected from the component depends on the component's albedo. An object's albedo is a quantity intrinsic to the external material or aggregate of materials, and is assumed to be constant in the near term².

Equation (4-4) is now re-written as (4-5), bearing these relationships in mind.

$$I_{RSO} \left[\frac{W}{SR} \right] = aA_P [m^2] \frac{1}{\pi} f_{SUN} \left[\frac{W}{SR m^2} \right] \cos \omega \cos \theta + aA_B [m^2] \frac{1}{\pi} f_{SUN} \left[\frac{W}{SR m^2} \right] \cos \psi \cos \eta \quad (4-5)$$

4.3 DERIVATION OF THE PROJECTED ALBEDO-AREA EQUATION

Multiplying (4-5) through by π , (4-6) is obtained.

$$\pi I_{RSO} \left[\frac{W}{SR} \right] = aA_P [m^2] f_{SUN} \left[\frac{W}{SR m^2} \right] \cos(\omega) \cos(\theta) + aA_B [m^2] f_{SUN} \left[\frac{W}{SR m^2} \right] \cos(\psi) \cos(\eta) \quad (4-6)$$

Now, in (4-7), solar flux is transformed into intensity on the Right Hand Side (RHS) by (4-2), where $|RS|$ is the length of the RSO-Sun vector in meters, as shown in Fig. 4-1.

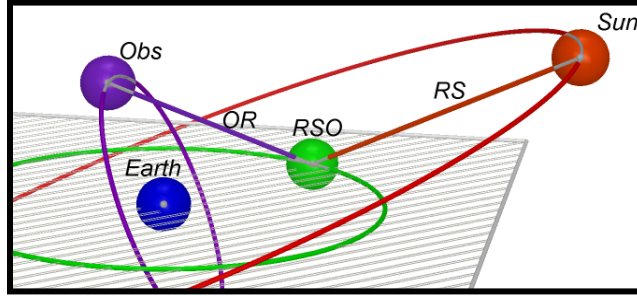


Fig. 4-1. OR and RS Vectors

$$\pi I_{RSO} \left[\frac{W}{SR} \right] = aA_P [m^2] \frac{I_{SUN} \left[\frac{W}{SR} \right]}{|RS|^2 [m^2]} \cos(\omega) \cos(\theta) + aA_B [m^2] \frac{I_{SUN} \left[\frac{W}{SR} \right]}{|RS|^2 [m^2]} \cos(\psi) \cos(\eta) \quad (4-7)$$

$$\pi I_{RSO} \left[\frac{W}{SR} \right] = \frac{I_{SUN} \left[\frac{W}{SR} \right]}{|RS|^2 [m^2]} (aA_P \cos(\omega) \cos(\theta) + aA_B \cos(\psi) \cos(\eta)) [m^2]$$

Multiplying through by the reciprocal, (4-8) is obtained.

$$\pi \frac{|RS|^2 [m^2]}{I_{SUN} \left[\frac{W}{SR} \right]} I_{RSO} \left[\frac{W}{SR} \right] = aA_P \cos(\omega) \cos(\theta) + aA_B \cos(\psi) \cos(\eta) [m^2] \quad (4-8)$$

$$\pi \frac{|RS|^2 [m^2] I_{RSO} \left[\frac{W}{SR} \right]}{I_{SUN} \left[\frac{W}{SR} \right]} = aA_P \cos(\omega) \cos(\theta) + aA_B \cos(\psi) \cos(\eta) [m^2]$$

The intensities (and their respective units) are now transformed into flux on the Left Hand Side (LHS) of (4-8) by (4-2), where $|OR|$ is the length of the Observer-RSO vector in meters, as shown in Fig. 4-1. Cancelling units on the LHS, (4-9) is obtained.

² We know that there are space aging effects that change the albedo over time.

$$\pi \frac{|RS|^2 [m^2] f_{RSO} \left[\frac{W}{sr m^2} \right] |OR|^2 [m^2]}{f_{SUN} \left[\frac{W}{sr m^2} \right] |RS|^2 [m^2]} = aA_P \cos(\omega) \cos(\theta) + aA_B \cos(\psi) \cos(\eta) [m^2] \quad (4-9)$$

↓

$$\pi \frac{|RS|^2 |OR|^2 f_{RSO}}{|RS|^2 f_{SUN}} [m^2] = aA_P \cos(\omega) \cos(\theta) + aA_B \cos(\psi) \cos(\eta) [m^2]$$

The ratio of fluxes on the LHS of (4-9) is transformed into an expression of apparent magnitudes by (4-3), and (4-10) is obtained.

$$\pi \frac{|RS|^2 |OR|^2}{|RS|^2} 10^{\frac{m_{SUN} - m_{RSO}}{2.5}} [m^2] = aA_P \cos(\omega) \cos(\theta) + aA_B \cos(\psi) \cos(\eta) [m^2] \quad (4-10)$$

Note the presence of $|RS|^2$ in both the numerator and the denominator of the LHS of (4-10). Rather than canceling these terms, however, $|RS|$ is fixed in the denominator to a constant value, the number of meters in an astronomical unit, denoted $|AU|$. As $|RS|$ and $|AU|$ are approximately equal, the effect of doing this is small. It serves the purpose, though, of taking into account the elliptical nature of the earth's orbit around the sun, which causes the distance from the earth to the sun to vary by as much as 3% from perihelion to aphelion.

The projected albedo-Area equation is now obtained in (4-11).

$$\pi \frac{|RS|^2 |OR|^2}{|AU|^2} 10^{\frac{m_{SUN} - m_{RSO}}{2.5}} [m^2] = aA_P \cos(\omega) \cos(\theta) + aA_B \cos(\psi) \cos(\eta) [m^2] \quad (4-11)$$

4.4 PROJECTED ALBEDO-AREA EQUATION IS NEARLY INDEPENDENT OF MODEL

Although a specific model was initially assumed on the RHS, namely the two-facet model described in Section 3.1, the result on the LHS of (4-11) would have been obtained regardless of the number of component terms in the model (i.e. the RHS). As long as the model consists of a sum of component Lambertian reflectances from the same source (in this particular case, the sun), it does not matter how many components the model possesses. Furthermore, although the trigonometric factors in this case are specific to the model, they are, for all intents and purposes, simply unit-less linear weights.

Although this equation is technically valid for a Lambertian reflectance only, analysis of data sets containing observations that exhibit specular glints has shown that, as long as the specular components are generally not dominant, the equation still yields useful results. For observations within an intense specular glint region, however, other considerations must be made and the underlying model adjusted. This is currently an active subject of study.

4.5 PROJECTED ALBEDO-AREA EQUATION, FINAL CONSIDERATIONS

There are now two equivalent expressions for the projected albedo area of a space object, denoted \widetilde{aA}_{RSO} in (4-12) and (4-13).

$$\widetilde{aA}_{RSO} = \pi \frac{|RS|^2 |OR|^2}{|AU|^2} 10^{\frac{m_{SUN} - m_{RSO}}{2.5}} [m^2] \quad (4-12)$$

$$\widetilde{aA}_{RSO} = aA_P \cos(\theta) \cos(\omega) + aA_B \cos(\psi) \cos(\eta) [m^2] \quad (4-13)$$

The quantity \widetilde{aA}_{RSO} changes with time, and it is a function of the geometry of the observation at any given time. The quantities aA_P and aA_B , on the other hand, are intrinsic to the specific space object and are not expected to change greatly over time. (Note that aA_B , the body component, displays slightly different behavior as the body is capable of self-occlusion, but this is addressed in the next section).

The value of \widetilde{aA}_{RSO} at any given observation may be determined from (4-12). Given enough of these observations, it is possible to construct a set of linear equations from (4-13), allowing a solution for the intrinsic panel and body albedo-Area components, aA_P and aA_B , to be determined. This derivation is presented in Section 6.0.

5.0 CLOSER EXAMINATION OF THE BODY COMPONENT

In Section 3.4, a model of the total reflected intensity was constructed, reprinted here in (5-1).

$$I_{RSO} = I_{PL} \cos(\omega) \cos(\theta) + I_{BL} \cos(\psi) \cos(\eta) [W/sr] \quad (5-1)$$

From this expression for the total reflected intensity, an expression for the total projected albedo-Area was derived in Section 4.0, reprinted here in (5-2).

$$\widetilde{aA}_{RSO} = \pi \frac{|RS|^2 |OR|^2}{|AU|^2} 10^{\frac{m_{SUN} - m_{RSO}}{2.5}} [m^2] = aA_P \cos(\theta) \cos(\omega) + aA_B \cos(\psi) \cos(\eta) [m^2] \quad (5-2)$$

Isolating the body's component, as expressed in the RHS of (5-2), the expression for the projected body albedo-Area is written in (5-3). (Recall that the trigonometric factors are explained in detail in Section 3.3).

$$\widetilde{aA}_B = aA_B \cos(\psi) \cos(\eta) [m^2] \quad (5-3)$$

The particulars of the body's reflectance are now described.

5.1 THE BODY AS A COMPLEX THREE DIMENSIONAL CONSTRUCT

While a solar panel is assumed to be nearly planar and is currently modeled as a single flat facet, the same model cannot be assumed equally valid for the body. The body, after all, is a complex, three dimensional construct, possessing multiple attachments for environmental sensing, data collection, transmission, etc. Consider, for instance, the following rendering of Galaxy 14, a typical geosynchronous communications satellite, shown next in Fig. 5-1.

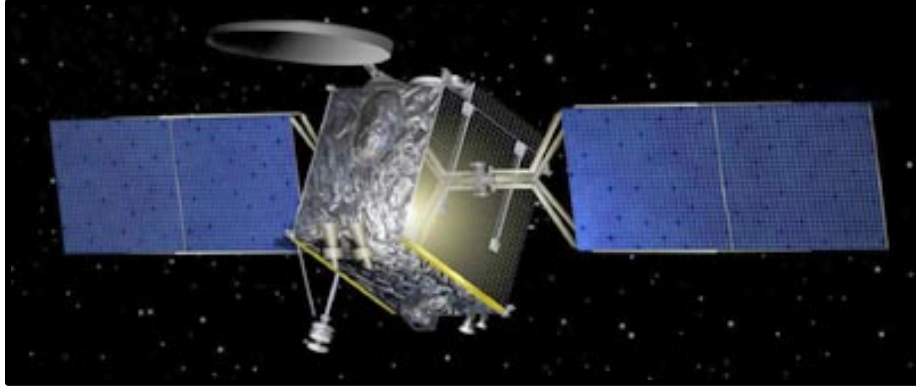


Fig. 5-1. Galaxy 14 Model [6]

5.2 THE BODY'S OBSERVABLE ALBEDO-AREA IS DEPENDENT ON POSE

As can be seen in Fig. 5-1, while the Galaxy 14 bus is generally cubical, it possesses a large, parabolic communications dish and a cover of crinkled Mylar. Now imagine observing Galaxy 14 in various poses relative to the sun and making photometric measurements of its solar reflectance. In one pose, the satellite may be positioned such that both the dish and the main body section are facing the sun head on, causing both sections to make a maximal contribution to the total observed reflectance. As the satellite orbits the earth, however, and its pose relative to the sun evolves, the satellite may be positioned such that the main body occludes the dish from the sun. In this instance, the dish would no longer be contributing to the body's total albedo-Area.

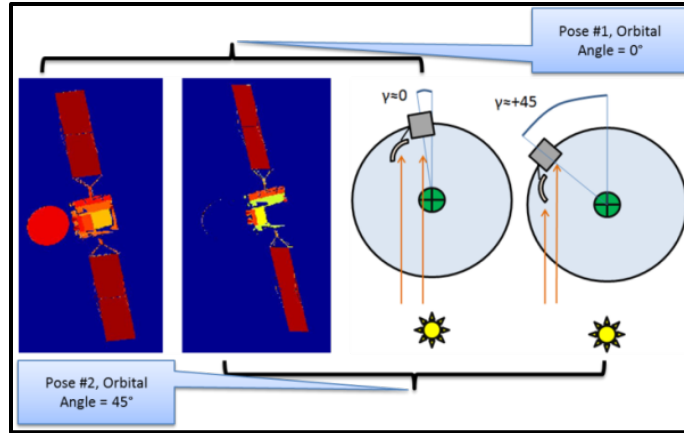


Fig. 5-2. Simulated Galaxy 14 Images in Different Poses³ and Notional Relationship with Orbital Angle

Consider Fig. 5-2, a notional rendering of two resolved thermal images of a Galaxy 14-like satellite in two different poses relative to the sun, measured in terms of the orbital angle γ (described in Section 3.3.2). For values of γ near zero, the dish and most of the nadir pointing features of the body are illuminated. As γ increases, however, a significant portion of the body falls into shadow, perhaps occluded from the sun by other features on the body, and the dish is completely in shadow. Therefore, while the albedo of the materials of the body remains unchanged in the near term, the *observable* albedo-Area of the body is dependent on the solar illumination that reaches the body, which in turn depends on the satellite's pose in relation to the sun, as measured by the orbital angle.

It is important to note that the change in the body's albedo-Area due to the pose is independent of the BRDF of the body's materials, i.e. *the ratio of outgoing to incoming solar radiation remains fixed for each part of the body*. This variation, rather, is due to the body's self-occlusion at certain poses with respect to the sun. Since such "dark" areas of the body can provide no information regarding its albedo and since self-occlusion depends on the changing pose, the body's intrinsic albedo-Area, in contrast to that of the panel, depends on the orbital angle at which it is observed.

5.3 EXPRESSING COMPONENT BODY ALBEDO-AREA AS A FUNCTION OF ORBITAL ANGLE

Consider the expression for the body's projected albedo-Area at a given observation from Equation (5-3). Although that expression contains only a single intrinsic albedo-Area term for the body, the body possesses an *observable intrinsic* albedo-Area that is different for each possible pose relative to the sun, as measured by orbital angle. A new expression for the body's projected albedo-Area is now constructed bearing this in mind.

First, the observable-intrinsic albedo-Area of the body at any given pose is expressed as a function of orbital angle γ . As this function depends on orbital angle, its domain is the same as the orbital angle's range: $(-\frac{\pi}{2}, \frac{\pi}{2})$. As ancillary body features tend to dominate along the orbital angle fringes, the domain is further restricted to $(-\frac{5\pi}{12}, \frac{5\pi}{12})$.

Next, the domain is discretized into $n = 10$ equal sub-intervals of $\frac{\pi}{12}$ (or 15°) each. Within each sub-interval, the body's albedo-Area is linearly interpolated according to Lagrange interpolation functions labeled as w_j . This allows for a piecewise continuous representation of the body contribution over the entire range of the domain.

Lastly, in addition to the $n = 10$ linearly interpolated terms, a spherical term B_{sph} is introduced to the body's model. This is the contribution that a Lambertian sphere of some given cross-sectional area would provide to the total observed albedo-Area of the body. These $n + 1 = 11$ terms ($n = 10$ linearly interpolated terms and 1 spherical term) now form the basis of the body's model. Equation (5-3) is now re-written as (5-4).

³ The two left panels in this figure contain images that were simulated by Kris Hamada (Pacific Defense Solutions) using the TASAT software at the request of the authors and courtesy of Paul Kervin (AFRL/RDSM). TASAT is Time-domain Analysis Simulation for Advanced Tracking.

$$\begin{aligned} \overline{aA_B} &= aA_B \cos(\psi)\cos(\eta) [m^2] \\ &\quad \downarrow \\ \overline{aA_B} &= \cos(\psi)\cos(\eta) \left(\sum_1^n (aA_{B_j} w_j(\gamma_j)) + aA_{B_{sph}} B_{sph} \right) [m^2] \end{aligned} \quad (5-4)$$

The observable-intrinsic albedo-Area of the body, then, as a function of orbital angle, is given by the vector shown in (5-5).

$$\overline{aA_B} = \begin{pmatrix} aA_{B_1} \\ \vdots \\ aA_{B_n} \\ aA_{B_{sph}} \end{pmatrix} \quad (5-5)$$

5.4 ADAPTING THE PROJECTED ALBEDO-AREA EQUATION TO THE BODY MODEL

The model for the body's projected albedo-Area shown in (5-4) is simply a sum of projected albedo-Areas, all of dimension length squared. In Section 4.0, the total projected albedo-Area equation was derived and reprinted in this section as (5-2). However, had the more complex expression of the body's albedo-Area shown in (5-4) been used on the RHS of the derivation, the same resulting LHS would have been obtained. The reason is each component albedo-Area of the body is assumed Lambertian (as in the derivation in Section 4.1) and is multiplied by same factor of $1/\pi$ (Section 2.3). Furthermore, each component albedo-Area is the result of the same underlying incident solar flux, and is thus proportional to the same solar constant (Section 4.2).

The total projected albedo-Area equation using the new model for the body is now written in (5-6).

$$\begin{aligned} \overline{aA_{RSO}} &= \\ [LHS] \pi \frac{|RS|^2 |OR|^2}{|AU|^2} 10^{\frac{m_{SUN}-m_{RSO}}{2.5}} [m^2] &= \\ [RHS] aA_P \cos(\theta)\cos(\omega) + \cos(\psi)\cos(\eta) \left(\sum_1^n (aA_{B_j} w_j(\gamma_j)) + aA_{B_{sph}} B_{sph} \right) [m^2] \end{aligned} \quad (5-6)$$

Now that the body's contribution is characterized more fully with respect to its complex nature, it is possible to construct a set of linear equations that will facilitate the decomposition of the total projected albedo-Area into its panel and body components.

6.0 DECOMPOSITION INTO PANEL AND BODY COMPONENT ALBEDO-AREAS

Up to this point, only the total projected albedo-Area has been considered. That is to say, only the LHS of (5-6) has been used. The decomposition of the total albedo-Area into its components, as seen in the RHS of (5-6), however, is necessary in order to characterize the space object using invariant features rather than features that vary depending on the time of observation [7]. In this section, the methodology employed to obtain this decomposition is described.

6.1 MOTIVATION FOR CURRENT DECOMPOSITION METHOD

In previous work, a decomposition method called *Point-Pairing* was described [3]. This method exploits geometric characteristics of observing conditions that have been specifically tasked to the sensor to meet certain criteria which cause the panel's contribution to the total projected albedo-Area to cancel. In the event that such sensor tasking is available, this method provides a straightforward approach to the decomposition of the aggregate photometric signature into its panel and body components.

A means by which to leverage serendipitous photometric observations that have *already* been collected by the sensor during the routine metrics mission, however, is desired. Exploiting observation data sets that might otherwise lie fallow, this method would provide great value by eliminating the need to task limited sensor resources. Furthermore, it would provide more timely results. Using observation data sets that already exist, after all, removes the need to wait for sensor tasking to be completed.

The method currently employed to decompose these serendipitous observation data sets into the panel and body components, called *Zero-Tasking*, is now described.

6.2 OUTLINE OF THE DECOMPOSITION METHOD, “ZERO-TASKING”

Consider a set observations obtained over a certain epoch of time.

For each observation i , the total projected albedo-Area is obtained from the LHS of (5-6). Next, the panel and body basis values are calculated, as shown in Tab. 1, from the RHS of (5-6). Note that j is the index of each linearly interpolated term for each observation i .

Tab. 1. Parameters for Zero Tasking

Total Projected aA Value, denoted $\overline{aA_{RSO_i}}$	$\pi 10^{\frac{m_{sun}-m_{RSO_i}}{2.5}} \frac{ \overline{OR_i} ^2 \overline{RS_i} ^2}{ AU ^2}$
Panel Basis Value, denoted \mathbf{p}_i	$\cos(\omega_i) \cos(\theta_i)$
10 Body Basis Function Values, denoted \mathbf{b}_{ij} An 11 th body term is the spherical component B_{sph}	$[\#1 - \#10] \cos(\psi_i) \cos(\eta_i) [w_{j=1}(\gamma_i), w_{j=2}(\gamma_i), \dots, w_{j=10}(\gamma_i)]$ $[\#11] B_{sph}$
Solution vector of component panel and body albedo-Areas that is sought, denoted $\overline{aA_x}$	$\begin{pmatrix} aA_p \\ aA_{B_1} \\ \vdots \\ aA_{B_n} \\ aA_{B_{sph}} \end{pmatrix}$

Once these parameters are computed, a system of linear equations based on (5-6) is constructed for the set of observations in each epoch. This linear system is then solved for the solution vector $\overline{aA_x}$ of component panel and body albedo-Areas.

First, the matrix of coefficients from the second and third rows of Tab. 1 denoted A in (6-1), is constructed.

$$A = \begin{pmatrix} \mathbf{p}_1 & \mathbf{b}_{11} & \dots & \mathbf{b}_{1j} & \mathbf{b}_{sph_1} \\ \vdots & \vdots & \ddots & \vdots & \vdots \\ \mathbf{p}_i & \mathbf{b}_{i1} & \dots & \mathbf{b}_{ij} & \mathbf{b}_{sph_i} \end{pmatrix} \quad (6-1)$$

Next, the vector of constants from the expression in the first row of Tab. 1 is constructed from the LHS of (5-6), denoted as $\overline{\mathbf{C}}$ in (6-2).

$$\overline{\mathbf{C}} = \begin{pmatrix} \overline{aA_{RSO_1}} \\ \vdots \\ \overline{aA_{RSO_i}} \end{pmatrix} \quad (6-2)$$

Next, in (6-3), a matrix equation is constructed from A and \vec{C} to solve for the solution vector \vec{aA}_x (shown in the last row of Tab. 1).

$$A \vec{aA}_x = \vec{C} \quad (6-3)$$

Before attempting to solve this equation, however, it is noted that the linear system is over-determined. That is to say that, since there are typically more observations made than variables to solve, there are more non-zero rows than non-zero columns in the matrix A . A basis pursuit technique is therefore employed, constructing the pseudo-inverse of A , denoted as $pinv(A)$, to solve for the solution vector \vec{aA}_x . The final expression for the decomposition of the component panel and body albedo-Areas is shown in (6-4).

$$\vec{aA}_x = pinv(A) \vec{C} \quad (6-4)$$

While the method of decomposition described in this section has yielded good results on both simulated and real data sets, it should be noted that this type of analysis (singular value decomposition) does not provide an exact solution to the over-defined system of equations in question. Such a system of equations may not, after all, have an exact solution. Instead, it provides an approximate solution vector with the smallest error possible. The chief advantage of this method, however, is that it assumes *no* special conditions on the observations and requires no special tasking of the sensor—hence the name *Zero-Tasking*. On the other hand, the decomposition could be combined with and enhanced by any other insight into the space object’s photometry that may be available, either serendipitously or specially tasked. For instance, if there happens to be a pair of observations in the data set that meets the geometric compatibility requirements necessary for one component’s contribution to cancel [3], the decomposition may be further refined.

7.0 CONCLUSIONS

In this paper we have provided an explanation of the physical and mathematical foundations used in extracting the albedo-Area from photometric data. We have shown the derivation of the calculations that decompose the total photometric signature into component panel and body albedo-Areas. The construction of the two-facet model was explained and an overview given of the geometry and the BRDF employed. The derivation of the total albedo-Area from its photometric signature was presented along with a method to decompose the total projected albedo-Area into the component panel and body albedo-Areas.

8.0 REFERENCES

1. Hall, D., *Optical CubeSat Discrimination*, AMOS Technical Conference, September 2008
2. Payne, T. E., Gregory, S. A., Luu, K., *SSA Analysis of GEOS Photometric Signature Classifications and Solar Panel Offsets*, AMOS Technical Conference, September 2006
3. Chaudhary, A.B., Payne, T., Gregory, S. and Dao, P., *Fingerprinting of Non-Resolved Three Axis Stabilized Space Objects Using a Two-Facet Analytical Model*, AMOS Technical Conference, 2011
4. Henden, Arne A., Kaitchuck, Ronald H., *Astronomical Photometry*, Appendix J, Willmann-Bell, Inc, 1990
5. Tatum, Jeremy, “Stellar Atmospheres,” <http://orca.phys.uvic.ca/~tatum/stellatm.html>, University of Victoria, 2011
6. Krebs, Gunter, “Gunter’s Space Page – Galaxy 12, 14, 15.” Retrieved from URL http://space.skyrocket.de/doc_sdat/galaxy-12.htm
7. Payne, T. E., Chaudhary, A. B., Gregory, S. A., Brown, J., Nosek, M., *Signature Intensity Derivative and its Application to Resident Space Object Typing*, AMOS Conference, September 2009